

# Dynamical system analysis of a data-driven model constructed by reservoir computing

Miki U. Kobayashi

*Faculty of Economics, Risho University, Tokyo 141-8602, Japan*

Kengo Nakai

*Faculty of Marine Technology, Tokyo University of Marine Science and Technology, Tokyo 135-8533, Japan*

Yoshitaka Saiki

*Graduate School of Business Administration, Hitotsubashi University, Tokyo 186-8601, Japan*

Natsuki Tsutsumi

*Faculty of Commerce and Management, Hitotsubashi University, Tokyo 186-8601, Japan*

(Dated: March 1, 2021)

This study evaluates data-driven models from a dynamical system perspective, such as unstable fixed points, periodic orbits, Lyapunov exponents, manifold structures, and statistical values. These dynamical characteristics can be reconstructed much more precisely by a data-driven model than by computing directly from training data. With this idea, we predict the laminar lasting time distribution of a particular macroscopic variable of chaotic fluid flow, which cannot be calculated from a direct numerical simulation of the Navier–Stokes equation because of its high computational cost.

**Introduction.** Reservoir computing, a brain-inspired machine-learning technique that employs a data-driven dynamical system, is effective in predicting time series and frequency spectra in chaotic behaviors, including fluid flow and global atmospheric dynamics [1–10]. Pathak *et al.* [3] examined the Lorenz system and the Kuramoto–Sivashinsky system and reported that the data-driven model obtained from reservoir computing could generate an arbitrarily long time series that mimics the dynamics of the original systems.

The extent to which a data-driven model using reservoir computing can capture the dynamical properties of original systems should be determined. Lu *et al.* [11] reported that a data-driven model has an attractor similar to that of the original system under an appropriate choice of parameters. Nakai and Saiki [12] confirmed that a single data-driven model could infer the time series of chaotic fluid flow from various initial conditions. Zhu *et al.* [13] identified some unstable periodic orbits of a data-driven model through delayed feedback control. They suggested that a data-driven model could reconstruct the attractor of the original dynamical system.

This Letter clarifies that a data-driven model using reservoir computing has richer information than that obtained from a training data, especially from dynamical system point of view, suggesting that dynamical properties of the original unknown dynamical system can be estimated by reservoir computing from a relatively short time series. Besides the invariant sets, such as fixed points and periodic orbits, the dynamical properties, such as Lyapunov exponents and manifold structures between stable and unstable manifolds, can be reconstructed by the data-driven model through reservoir computing, even if the system does not have structural

stability.

We mainly deal with the Lorenz system [14]:

$$\frac{dx}{dt} = 10(y - x), \quad \frac{dy}{dt} = rx - y - xz, \quad \frac{dz}{dt} = xy - \frac{8}{3}z, \quad (1)$$

and will be denoted as the actual Lorenz system in this Letter. A data-driven model is constructed from a short time training data created from (1), the method of which is explained later. Two different parameter values of  $r$  are considered. One of the parameters ( $r = 28$ ) has hyperbolic dynamics, whereas the other ( $r = 60$ ) generates dynamics with tangencies between stable and unstable manifolds [15]. The latter property is one of the two primary sources for the breaking structural stability [16], which often appears in the real-world physical phenomena. As an application of the obtained knowledge, this study examines high-dimensional chaotic fluid flow to determine if the laminar lasting time distribution can be predicted using the data-driven model constructed from short training time-series data.

**Reservoir computing.** A reservoir is a recurrent neural network whose internal parameters are not adjusted to fit the data in the training process [17, 18]. The reservoir can be trained by feeding it an input time series and fitting a linear function of the reservoir state variables to the desired output time series. We do not use a physical knowledge in constructing a model. The data-driven model using reservoir computing we study is the following:

$$\begin{cases} \mathbf{u}(t) = \mathbf{W}_{\text{out}}\mathbf{r}(t), \\ \mathbf{r}(t + \Delta t) = (1 - \alpha)\mathbf{r}(t) + \alpha \tanh(\mathbf{A}\mathbf{r}(t) + \mathbf{W}_{\text{in}}\mathbf{u}(t)), \end{cases} \quad (2)$$

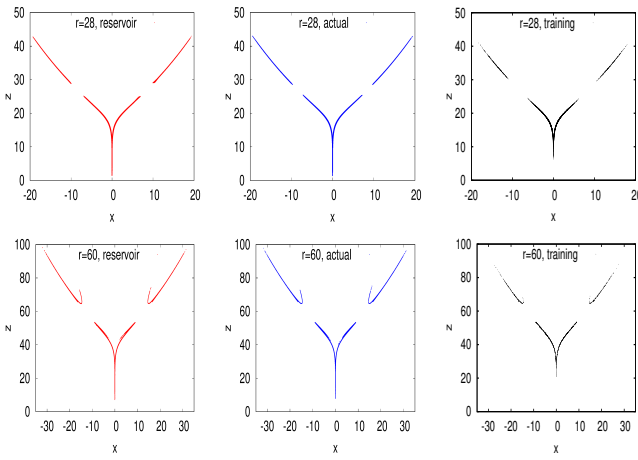


FIG. 1. **Poincaré section-like plots** ( $r = 28$  (top) and  $60$  (bottom)). The sets of points  $(x, z)$ : along a trajectory of the data-driven model using reservoir computing and along a long trajectory of the actual Lorenz system and along a short trajectory used for the training data are plotted when  $|x - y| < \epsilon_p$ , where  $\epsilon_p = 0.05$ . The time lengths of the three trajectories are  $T = 10^6$ ,  $10^6$ , and  $5000$ , respectively.

where  $\mathbf{u}(t) \in \mathbb{R}^M$  is a vector-valued variable, the component of which is denoted as an output variable;  $\mathbf{r}(t) \in \mathbb{R}^N$  ( $N \gg M$ ) is a reservoir state variable;  $\mathbf{A} \in \mathbb{R}^{N \times N}$ ,  $\mathbf{W}_{\text{in}} \in \mathbb{R}^{N \times M}$ , and  $\mathbf{W}_{\text{out}} \in \mathbb{R}^{M \times N}$  are matrices;  $\alpha$  ( $0 < \alpha \leq 1$ ) is a coefficient;  $\Delta t$  is a time step. We define  $\tanh(\mathbf{q}) = (\tanh(q_1), \tanh(q_2), \dots, \tanh(q_N))^T$ , for a vector  $\mathbf{q} = (q_1, q_2, \dots, q_N)^T$ , where  $T$  represents the transpose of a vector. We determine  $\mathbf{W}_{\text{out}}$  using training time series data  $\{\mathbf{u}(l\Delta t)\}_{l=0}^{L-1}$ . More details can be found elsewhere [6].

In this Letter we evaluate a data-driven model (2) constructed using short training time series data from a dynamical system perspective. The main focus is on the properties in the space of output variables (corresponding to  $x$ ,  $y$ , and  $z$  for the case of the Lorenz system), which compare them with those of the actual system.

**Poincaré section-like plots.** The Poincaré section of the data-driven model of the Lorenz system has been studied [3]. We compare the shape and size of the attractor of a data-driven model (2) with those of the attractor of the actual Lorenz system (1), and also with those of the set of points along the training time series data. Figure 1 presents their Poincaré section-like plots for  $r = 28$  and  $60$ . For each of the two parameter cases, a set of trajectory points generated from the data-driven model seem to coincide with the chaotic attractor of the actual Lorenz system. Furthermore, the data-driven model has an attractor which is significantly larger than the set of training data used to construct the model.

**Density distribution.** The density distribution of  $x$  variable along a trajectory of the data-driven model is presented in Fig. 2. We compare the distribution with that obtained from the trajectory of the actual Lorenz

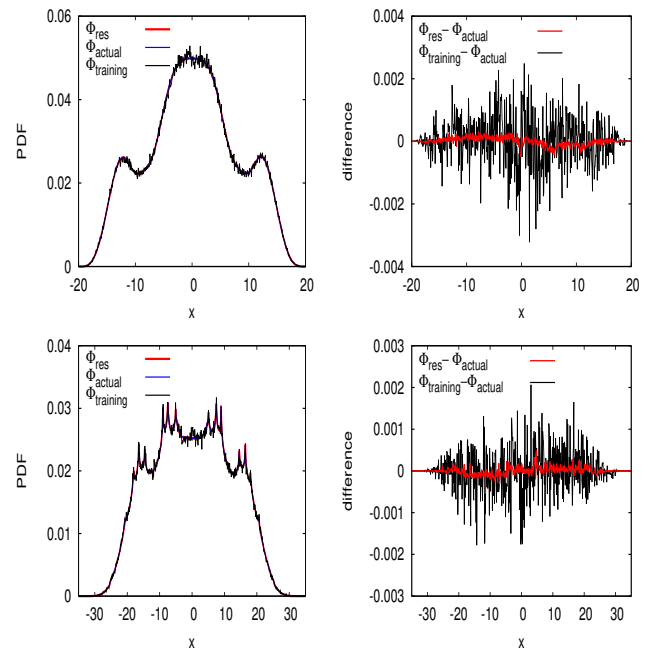


FIG. 2. **Density distributions of a variable** ( $r = 28$  (top) and  $r = 60$  (bottom)). The density distribution of the  $x$  variable calculated from a length  $T = 10^6$  trajectory of the data-driven model by reservoir computing ( $\Phi_{\text{res}}$ ) is plotted together with that computed from the length  $T = 10^6$  long trajectory of the actual Lorenz system ( $\Phi_{\text{actual}}$ ) and the length  $T = 5000$  short trajectory ( $\Phi_{\text{training}}$ ) used as training data for constructing the data-driven model. The difference in the distributions are shown on the right. The average  $\bar{x}$  and the standard deviation  $\sigma$  of the density distribution are as follows:  $(\bar{x}, \sigma) = (-0.004, 7.924)$  for the data-driven model, and  $(0.009, 7.925)$  for the Lorenz system with  $r = 28$ ;  $(\bar{x}, \sigma) = (-0.018, 12.092)$  for the data-driven model, and  $(-0.018, 12.091)$  for the Lorenz system with  $r = 60$ .  $\int |\Phi_{\text{res}} - \Phi_{\text{actual}}| dx / \int |\Phi_{\text{training}} - \Phi_{\text{actual}}| dx \approx 1/8$  for  $r = 28$ , and  $\approx 1/6$  for  $r = 60$ .

system (1) and that calculated directly from the training data. The distribution of the actual Lorenz system can be captured by employing the data-driven model. Remarkably, the distribution with a singular structure [19] in  $r = 60$  can be recovered using the data-driven model.

**Fixed points and their stabilities.** Fixed points, which are fundamental structures of dynamical systems, are examined. We identify fixed points in the space of the output variables directly, even though they were identified through the fixed points in the space of the reservoir state variables using the directional fibers method [20]. We also study the stability of each fixed point in the space of output variables. For the data-driven model we consider a point  $\mathbf{x}^* = (x^*, y^*, z^*)$  as a fixed point, when the following condition is satisfied:  $\delta = \max_{n \in [0, n_0]} \|\mathbf{x}^* - \psi_{\mathbf{x}^*}(n\Delta t)\|_{l^2} < \epsilon_0$  for some  $\epsilon_0$  sufficiently small and for some  $n_0$  sufficiently large, where  $\psi_{\mathbf{x}^*}(n\Delta t)$  is the point iterated  $n$  times from  $\mathbf{x}^*$  by the data-driven model with

	$L_{\text{res}}$	$R_{\text{res}}$	$O_{\text{res}}$	$L_{\text{actual}}$	$R_{\text{actual}}$	$O_{\text{actual}}$
$x^*$	-8.47	8.50	0.04	-8.49	8.49	0.00
$y^*$	-8.47	8.50	0.02	-8.49	8.49	0.00
$z^*$	27.04	27.01	0.54	27.00	27.00	0.00
$\Lambda_1$	$0.09 + 10.19i$	$0.10 + 10.21i$	11.67	$0.09 + 10.20i$	$0.09 + 10.20i$	11.83
$\Lambda_2$	$0.09 - 10.19i$	$0.10 - 10.21i$	-2.66	$0.09 - 10.20i$	$0.09 - 10.20i$	-2.67
$\Lambda_3$	-13.84	-13.86	-22.68	-13.85	-13.85	-22.83

TABLE I. **Coordinates and eigenvalues of the Jacobian matrix at each of the three fixed points.**  $L_{\text{res}}$ ,  $R_{\text{res}}$ , and  $O_{\text{res}}$  are fixed points of the data-driven model, whereas  $L_{\text{actual}}$ ,  $R_{\text{actual}}$ , and  $O_{\text{actual}}$  are fixed points of the actual Lorenz system with  $r = 28$ . The coordinates  $(x^*, y^*, z^*)$  and the eigenvalues  $(\Lambda_1, \Lambda_2, \Lambda_3)$  of the Jacobian matrix at each fixed point of the data-driven model are close to those of the corresponding fixed point of the actual Lorenz system.

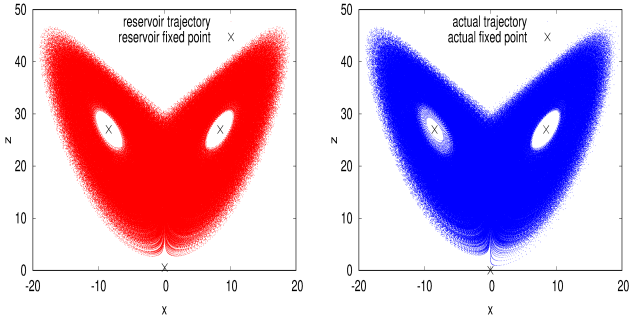


FIG. 3. **Fixed points.** The three fixed points  $(x^*, y^*, z^*)$  of the data-driven model (left) and those of the actual Lorenz system (right) are plotted together with the trajectory points with the time length  $T = 10^4$ . The three fixed points of the data-driven model are close to those of the actual Lorenz system, despite the fixed points being outside the training data, which is part of the actual trajectory. See the coordinates and the eigenvalues of the Jacobian matrix at each fixed point in Table I.

the time step  $\Delta t$ . For the computation of a trajectory from a given point  $\mathbf{x}^*$  of the data-driven model, reservoir state vector  $\mathbf{r}(0)$  is determined to correspond to  $\mathbf{x}^*$  by the pre-iterates. The echo state property [17] in which our choice of parameters in the data-driven model (2) is satisfied guarantees that for each  $\mathbf{x}^*$ , the corresponding reservoir state vector is determined uniquely. Table I lists the obtained coordinates of the three fixed points,  $L_{\text{res}}$ ,  $R_{\text{res}}$  and  $O_{\text{res}}$ , together with those of the actual Lorenz system. We fix  $(\epsilon_0, n_0) = (0.01, 10000)$  for  $L_{\text{res}}$  and  $R_{\text{res}}$ , and  $(\epsilon_0, n_0) = (1, 30)$  for  $O_{\text{res}}$ . Figure 3 shows the fixed points together with the trajectory points. Table I also lists the eigenvalues of the Jacobian matrix at each fixed point. The values are obtained from the estimated formula of the Jacobian matrix described later for calculating the Lyapunov exponents and vectors.

**Periodic trajectory.** Periodic orbits are also the fundamental structures of dynamical systems. We confirm that the data-driven model of discrete time has a periodic orbit-like trajectory that travels near the corresponding periodic orbit of the actual Lorenz system (1) of continuous time. We call  $\{\psi_{\mathbf{x}(0)}(n\Delta t)\}_{n \in [0, n_p]}$  a peri-

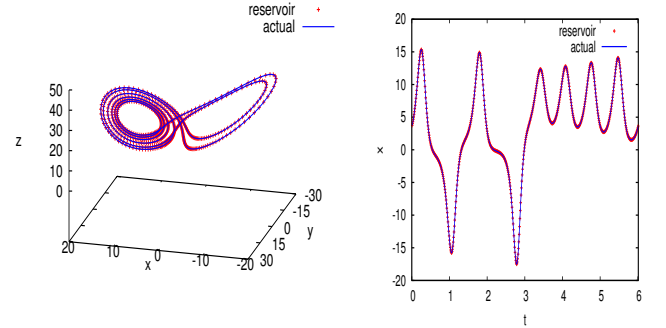


FIG. 4. **A periodic orbit-like trajectory.** A periodic orbit-like trajectory obtained from the data-driven model is plotted together with the corresponding periodic orbit (period  $T_p = 5.9973192969$ ) of the actual Lorenz system with  $r = 28$  (left), and their time developments of the  $x$  variable (right).

$r$	$\lambda_{\text{res}}^{(1)}$	$\lambda_{\text{res}}^{(2)}$	$\lambda_{\text{res}}^{(3)}$	$D_{\text{res}}^{KY}$	$\lambda_{\text{actual}}^{(1)}$	$\lambda_{\text{actual}}^{(2)}$	$\lambda_{\text{actual}}^{(3)}$	$D_{\text{actual}}^{KY}$
28	0.905	0.001	-14.574	2.06	0.905	0.001	-14.571	2.06
60	1.397	0.001	-15.065	2.09	1.403	0.001	-15.070	2.09

TABLE II. **Lyapunov exponents and Lyapunov dimensions.** Lyapunov exponents of the data-driven model using reservoir computing  $(\lambda_{\text{res}}^{(1)}, \lambda_{\text{res}}^{(2)}, \lambda_{\text{res}}^{(3)})$  and those of the actual Lorenz system  $(\lambda_{\text{actual}}^{(1)}, \lambda_{\text{actual}}^{(2)}, \lambda_{\text{actual}}^{(3)})$  are listed. The values are computed using the four-stage and fourth-order Runge-Kutta method with time step  $4\Delta t$  from the points along an orbit trajectory and the estimated Jacobian matrices. The Lyapunov dimensions  $D_{\text{res}}^{KY}$  for the data-driven model and  $D_{\text{actual}}^{KY}$  for the actual Lorenz system are estimated from the Kaplan-Yorke formula [21].

odic orbit-like trajectory, if the following value is sufficiently small:  $\delta_p = \max_{n \in [0, n_p]} \|\mathbf{x}(n\Delta t) - \psi_{\mathbf{x}(0)}(n\Delta t)\|_{l^2}$ , where  $\mathbf{x}(0)$  is a point on the corresponding periodic orbit with period  $T_p$  of the actual Lorenz system (1),  $n_p$  is the smallest integer satisfying  $n_p\Delta t \geq T_p$ . Among the periodic orbit-like trajectories of the data-driven model corresponding to the 50 periodic orbits with low periods,  $\delta_p < 0.1$  for 40 cases and  $\delta_p < 0.4$  for the other 10 cases. Figure 4 gives an example of a periodic orbit-like trajectory, which has the largest value of  $\delta_p$  among the 50 periodic orbits with low periods.

**Lyapunov exponents and Lyapunov vectors.** The Lyapunov exponents are used to evaluate the degree of instability and estimate the Lyapunov dimension of a dynamical system. In some studies, the Lyapunov exponents of a data-driven model by reservoir computing were calculated in the space of  $N$ -dimensional reservoir state variables [3, 4, 22, 23]. To the best of the authors' knowledge, they have not been computed only in a space of output variables.

In this Letter, an attempt is made to compute Lyapunov exponents in the space of output variables. The results are compared with those of the actual Lorenz system (1) for two sets of parameters. In this computa-

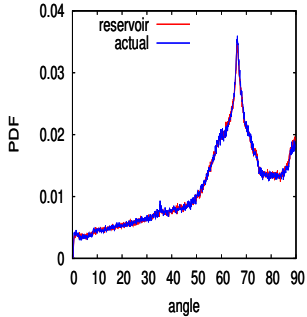
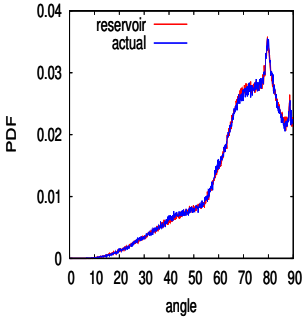


FIG. 5. **Distribution of the angle between stable and unstable manifolds** ( $r = 28$  (left) and  $r = 60$  (right)). The density distribution of the manifold angles (degree) at points along a trajectory is shown for a data-driven model using reservoir computing together with that of the actual Lorenz system.

tion the discrete time trajectory points of a data-driven model are considered samples of the continuous time trajectory. Table II shows the agreement of the Lyapunov exponents and the Lyapunov dimensions. We also compute (co-variant) Lyapunov vectors, which measure the degree of hyperbolicity by calculating the angle between the stable and unstable manifolds at some trajectory point [24]. The Lyapunov exponents and the Lyapunov vectors for the data-driven model are obtained from the Jacobian matrices estimated numerically from the trajectory points in the space of output variables [25].

**Manifold structure and Tangency.** Using the computed Lyapunov vectors we investigate the manifold structures of the data-driven model, particularly the degree of hyperbolicity and the tangencies between the stable and the unstable manifolds. We consider the Lorenz system of  $r = 28$  without tangencies and of  $r = 60$  with tangencies for the comparison [15]. Figure 5 shows the probability density function of an angle between a tangent vector of a stable manifold and that of an unstable manifold along an orbit trajectory for each of the actual system and the data-driven model. For each case of the parameters,  $r = 28$  and  $r = 60$ , the angle distributions are quite similar in shape, indicating that the data-driven model can reconstruct the manifold structures. Moreover, Fig. 5 (right) suggests that the data-driven model can represent a non-hyperbolic structure with tangencies between stable and unstable manifolds.

**Laminar lasting time distribution of chaotic fluid flow.** Applying the knowledge obtained above for the Lorenz system, we study laminar lasting time distribution of a macroscopic quantity of chaotic fluid flow in three dimensions under periodic boundary conditions [6, 12]. The distribution shown in Fig. 6 is generated from the very long trajectory of the data-driven model constructed by reservoir computing with a rela-

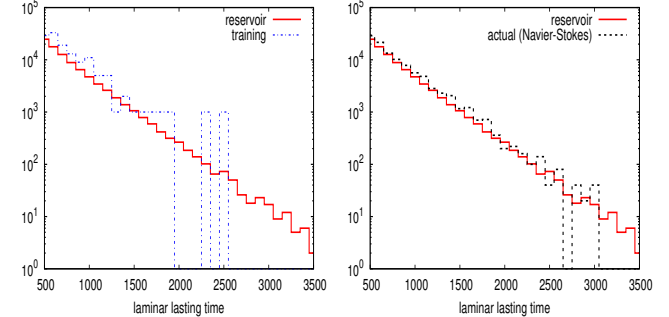


FIG. 6. **Laminar lasting time distribution of a fluid flow.** The laminar lasting time normalized distribution of a certain energy function  $E(t)$  of a fluid variable (corresponding to  $\tilde{E}(3, t)$  in [6]) estimated from the trajectory of the data-driven model ( $T_0 = 2 \times 10^8$ ) is shown together with that from the short time training time series data ( $T = 0.001 \times T_0$ ) (left) and with that by a long time actual time series data ( $T = 0.05 \times T_0$ ) (right). The training data and actual data are calculated from a direct numerical simulation of the Navier–Stokes system.  $E(t)$  is the normalized variable (average 0, standard deviation 1) and we consider the state is laminar when  $|E(t)| < 1.8$ .

tively low computational cost. The detailed macroscopic dynamical structures can be determined using the data-driven model constructed from time series data without referring to microscopic behaviors. We hardly obtain these structures from a direct numerical simulations of the Navier–Stokes equation because of the high computational cost. See the discrepancy in the distributions in Fig. 6 (right).

**Acknowledgements.** YS was supported by the JSPS KAKENHI Grant No.17K05360 and No.19KK0067. KN was supported by the Project of President Discretionary Budget of TUMST. Part of the computation was supported by JHPCN (jh200020), HPCI (hp200104), and the Collaborative Research Program for Young · Women Scientists of ACCMS and IIMC, Kyoto University.

---

[1] D. Verstraeten, B. Schrauwen, M. D’Haene, and D. A. Stroobandt, *Neural Networks* **20**, 391 (2007).  
[2] Z. Lu, J. Pathak, B. Hunt, M. Girvan, R. Brockett, and E. Ott, *Chaos* **27**, 041102 (2017).  
[3] J. Pathak, Z. Lu, B. Hunt, M. Girvan, and E. Ott, *Chaos* **27**, 121102 (2017).  
[4] J. Pathak, B. Hunt, M. Girvan, Z. Lu, and E. Ott, *Phys. Rev. Lett.* **120**, 024102 (2018).  
[5] P. Antonik, M. Gulina, J. Pauwels, and S. Massar, *Phys. Rev. E* **98**, 012215 (2018).  
[6] K. Nakai and Y. Saiki, *Phys. Rev. E* **98**, 023111 (2018).  
[7] T. Arcaman, I. Szunyogh, J. Pathak, A. Wikner, B. R. Hunt, and E. Ott, *Geophys. Res. Lett.* **47**, e2020GL087776 (2020).

- [8] S. Pandey and J. Schumacher, Phys. Rev. Fluids **5**, 113506 (2020).
- [9] Y. Huang, L. Yang, and Z. Fu, Earth System Dynamics **11**, 835 (2020).
- [10] L.-W. Kong, H.-W. Fan, C. Grebogi, and Y.-C. Lai, Phys. Rev. Res. **3**, 013090 (2021).
- [11] Z. Lu, B. R. Hunt, and E. Ott, Chaos **28**, 061104 (2018).
- [12] K. Nakai and Y. Saiki, Discrete Contin. Dyn. Syst. S **14**, 1079 (2021).
- [13] Q. Zhu, H. Ma, and W. Lin, Chaos **29**, 093125 (2019).
- [14] E. Lorenz, J. At. Sci. **20**, 130 (1963).
- [15] Y. Saiki and M. U. Kobayashi, JSIAM Lett. **2**, 107 (2010).
- [16] C. Bonatti, L. Díaz, and M. Viana, *Dynamics Beyond Uniform Hyperbolicity* (Springer-Verlag, Berlin, 2005).
- [17] H. Jaeger, GMD Report **148**, 13 (2001).
- [18] H. Jaeger and H. Haas, Science **304**, 78 (2004).
- [19] S. M. Zoldi, Phys. Rev. Lett. **81**, 3375 (1998).
- [20] S. Krishnagopal, G. Katz, M. Girvan, and J. Reggia, in *2019 International Joint Conference on Neural Networks (IJCNN)* (IEEE, 2019) pp. 1–8.
- [21] J. Kaplan and J. Yorke, in *Functional differential equations and approximation of fixed points (Proc. Summer School and Conf., Univ. Bonn, Bonn, 1978)*, Lecture Notes in Math., Vol. 730 (Springer, Berlin, 1979) pp. 204–227.
- [22] C. Gallicchio, A. Michel, and L. Silvestri, Neurocomputing **298**, 34 (2018).
- [23] V. Pyragas and K. Pyragas, Phys. Lett. A **384**, 126591 (2020).
- [24] F. Ginelli, P. Poggi, A. Turchi, H. Chaté, R. Livi, and A. Politi, Phys. Rev. Lett. **99**, 130601 (2007).
- [25] K. Nakai, Y. Saiki, and N. Tsutsumi, in preparation (2021).